IEEE Photonics Journal
An IEEE Photonics Society Publication

Open Access

Investigation of Enhanced Transmission and Beaming Effect Through an InSb Subwavelength Grating With a Slit at the Terahertz Range

Volume 12, Number 1, February 2020

Xinyi Liu
Yan Liu
Cizhe Fang
Genquan Han, *Member, IEEE*
Yue Hao, *Senior Member, IEEE*

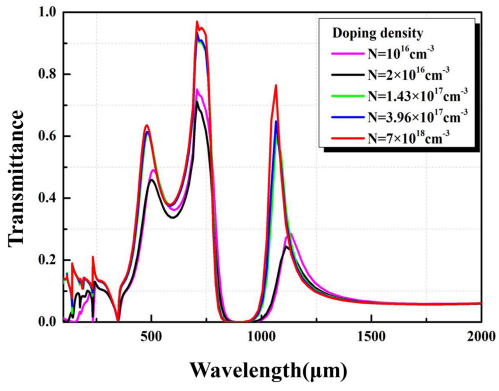

(a)

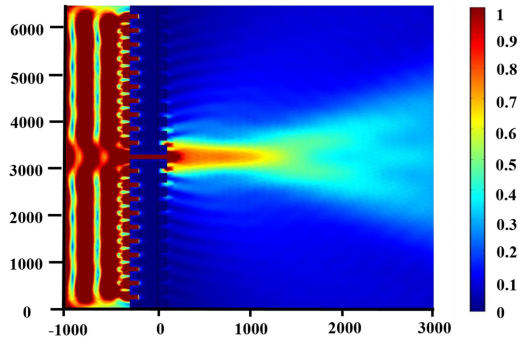

(b)

DOI: 10.1109/JPHOT.2019.2957533

Investigation of Enhanced Transmission and Beaming Effect Through an InSb Subwavelength Grating With a Slit at the Terahertz Range

Xinyi Liu, Yan Liu, Cizhe Fang, Genquan Han, *Member, IEEE*, and Yue Hao, *Senior Member, IEEE*

Wide Bandgap Semiconductor Technology Disciplines State Key Laboratory, School of Microelectronics, Xidian University, Xi'an 710071, China

DOI:10.1109/JPHOT.2019.2957533

Manuscript received November 20, 2019; accepted November 30, 2019. Date of publication December 4, 2019; date of current version January 7, 2020. This work was supported in part by the National Key Research and Development Project under Grants 2018YFB2200500 and 2018YFB2202800 and in part by the National Natural Science Foundation of China under Grants 61534004, 91964202, 61874081, and 61851406. Corresponding author: Yan Liu (e-mail: xdliuyan@xidian.edu.cn).

Abstract: In this paper, we demonstrate the feasibility of realizing the extraordinary optical transmission (EOT) and the collimated beaming effect through InSb grating, which has a subwavelength slit surrounded by a finite array of grooves at both sides of the surface. Firstly, we investigate the transmission properties of the structure by changing the temperature and doping concentration of InSb, and the optimized transmission can reach almost 95%. Besides, it is verified that the transmission is mainly controlled by the pattern on the input corrugation with the variable dimension parameters. At last, the properties of the beaming intensity and focal length are thoroughly analyzed with the variation of the number and depth of the grooves on the output corrugation. These results provide a new plasmonic solution for controlling light in a variety of integrated optical components in the terahertz range.

Index Terms: Doped InSb, extraordinary optical transmission, beaming effect.

1. Introduction

With the in-depth study of the Surface Plasmon Polaritons (SPPs) theory, a lot of unsolved optical problems have been explained and settled and the great potential of SPPs in the application of various optical components was revealed. SPPs are electromagnetic waves bounded to the interface between a conductor and a dielectric [1], which have opposite permittivities. Numerous studies of the application of SPPs are focusing on the excitation and guiding along with a planar interface. For example, the control over the propagation of the waves for waveguiding applications was achieved by surface patterning [2], or the special phenomenon of rainbow trapping has paved the way for the applications of SPPs in improving the performance of optical switching or optical signal procession [3]. All of the above researches are focusing on the active control of the SPP propagation along the surface grooves in the horizontal direction. In addition, it is also worth noting that there are many applications of SPPs in the perpendicular direction, which focus on the transmission of electromagnetic energy through the thin metallic film. Since Ebbesen first reported the

extraordinary optical transmission (EOT) phenomena through a two-dimensional (2-D) hole array perforated on a silver screen in 1998 [4], considerable researches on the optical properties of this periodic subwavelength structure have been conducted [5]–[18]. The transmittance of light passing through the periodic structure surrounded by surface corrugation has been studied extensively. If the film is patterned with a regular array of holes, or surface corrugations surrounding a single slit, the enhanced transmission phenomena and directional beaming effect will be observed. For example, the study of the optical transmission properties of a single slit in a corrugated metal film has been described. And the enhancements of light by up to 2 orders of magnitude was achieved by modulating the groove parameters [19]. It is now a well-established agreement that the large transmission enhancement is related to two types of transmission resonances: coupled surface plasmon polariton (SPP) resonances and slit waveguide modes [11], [12], [19]–[21], which satisfy the conservation of energy and momentum on the surface [22]. Similarly, Lezec first described the highly directional emission with a narrow beaming angle on a regular grating structure in 2002 [6]. A bull's eye structure surrounding a circular subwavelength aperture and a single slit surrounded by parallel grooves were introduced to channel light in a well-defined direction as a collimate beam. Since then, abundant researches have been done on the grating structure with periodic grooves on the output surface to investigate the beaming effect [23]–[25]. This effect can be understood as the formation of surface electromagnetic (EM) resonances on the output surface [26]. While the properties of the transmission can be controlled basically by the phase-matching condition imposed by the pattern on the input corrugation, the angular intensity distribution of the emitted beam is governed by the pattern on the output corrugation. These two combined abilities make this type of structure a good candidate to play a major role in many optoelectronic applications, such as molecular sensing, spectroscopy and stand-alone photonic devices.

Metals, as a conventional plasmonic material, excite well-confined SPPs only at visible and near-infrared frequencies for its large free electron density $n_e \approx 10^{23}$ cm^{-3}. At far-infrared frequencies in the THz regime, the complex dielectric constant of metal is very large due to their high carrier density, which causes a serious surface impedance imbalance, and makes the lower field penetration in the metal, hence, resulting in the limitation on the optical field [27]. For the coupling between THz radiation and metal's free electrons is poor, it is difficult to observe significant SPPs characteristics and transmission enhancement, which is believed to be a limitation for the scalability of metal within THz spectra [22]. Therefore, researchers turned to other materials for exploring SPPs phenomenon at THz range. Numerous researches show that the dielectric constant of the doped semiconductor in the THz is about 10^2, and it is close to that of the metal in the visible optical band, which is lower than 10^2. This feature resulting in similar optical properties between them [28]. The metallic characteristic of doped semiconductors such as silicon and InSb at low frequencies makes it possible to excite SPPs at mid-infrared, THz, and microwave frequencies. The transmission through square gratings of apertures structured in doped silicon was widely investigated [29]–[31]. Simultaneously, active control of SPPs excitation can be achieved by adjusting carrier concentration and mobility of InSb. An additional advantage of InSb material is that their dielectric constant can be also tuned by changing temperature or doping [32]. Compared with metals, flexible tuning also provides processing convenience for the applications of InSb SPPs excitation in the THz frequency.

In this paper, we demonstrate the feasibility of realizing the extraordinary optical transmission and the collimated beaming effect through a subwavelength slit aperture surrounded by a finite array of grooves at both sides of the surface using InSb instead of metal. Optical characteristics of the grating structure are thoroughly analyzed by tuning the geometrical parameters of both sides and displayed by the transmittance spectrums and the optical field intensity distribution. The greatly enhanced transmission was achieved by changing the temperature, doping concentration and the geometrical parameters of the input surface of the structure while the detail of the beaming mechanism was also investigated by tuning the output surface. These features make this structure an excellent candidate for plasmonic components in all-optical and optoelectronic fields.

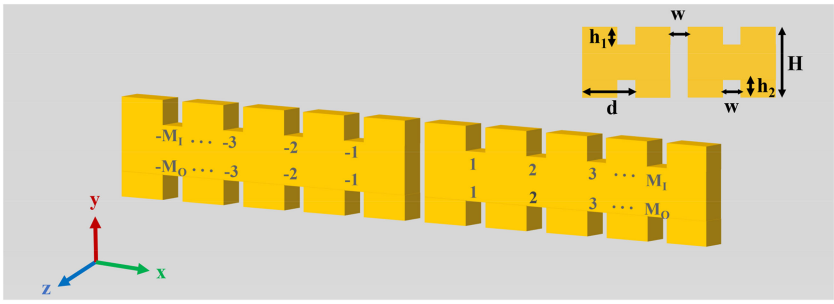

Fig. 1. 3D schematic of the designed slit aperture surrounded by a finite array of grooves with InSb.

2. Device Structure

In order to investigate the SPPs properties of the EOT phenomenon and the beaming effect of the InSb grating waveguide at the same time, the structure we used is shown in Fig. 1. The slit aperture is surrounded by a finite array of grooves on both sides of the surface. The finite-difference-time-domain (FDTD) simulation methods are carried out to obtain the transmittance of the structure by tuning the input surface. In the simulation, the incident light is a TM polarized wave propagating along with the *y* direction, and the direction of the electric field E and magnetic field H is *y* and *z*, respectively. Therefore, the thickness of the InSb strip along the *z*-direction is negligible. The letter *d* represents the period of the structure, h_1 and h_2 are marked as the depth of the input and output grooves respectively, *H* represents the height of the grating and is set to be 400 μm. We set the width of the grooves and the slit to be the same value, which is represented by w. The number of the grooves to one side of the central slit at the input surface is represented by M_{I}, and the number of the grooves to one side of the central slit at the output surface is represented by M_{O}. In our work, the transmittance properties and the focusing effect of the grating are thoroughly explored by preparing and analyzing a variety of combinations of parameters for this 3-dimensional array. Such a grating structure could be fabricated using the electron beam lithography (EBL) and the inductively coupled plasma (ICP) dry etching processes. First, the doped Insb material could be obtained through ion implantation technology. Then the EBL process and poly(methyl methacrylate) (PMMA) were used to prepare the mask of the device. And the grating could be patterned through ICP dry etching process. Nowadays, the semiconductor manufacturing process has entered the nanometer scale, therefore the influence of fabrication tolerance on the performance of such micrometer scale device could be negligent.

3. Results and Discussion

The doped InSb not only has the metallic characteristics at low frequencies that can excite SPPs at mid-infrared, THz, and microwave frequencies, but also has a great advantage over metals, which is due to that its permittivity can be easily modified by the temperature and the doping concentration, and then affects the SPPs characteristics and the subwavelength transmission. Taking into account this property, we first investigate the effect of these two factors on transmission. InSb is characterized by the complex permittivity ($\varepsilon = \varepsilon' + \varepsilon''$) with a negative ε'. It has been verified from the optical experiments that more pronounced enhancement of the transmission occurs when ε' is greater than ε'' [33]. The permittivities we used in the calculation are obtained from Fig. 2(a), which provides the main parameters for the Drude model of doped InSb. The Drude mode of doped InSb is well described as follows [22], [34]:

$$\varepsilon(\omega) = \varepsilon_{\infty}\left(1 - \frac{\omega_p^2}{\omega^2 + \tau^{-2}} + i\frac{\omega_p^2\tau^{-1}}{\omega\left(\omega^2 + \tau^{-2}\right)}\right) \tag{1}$$

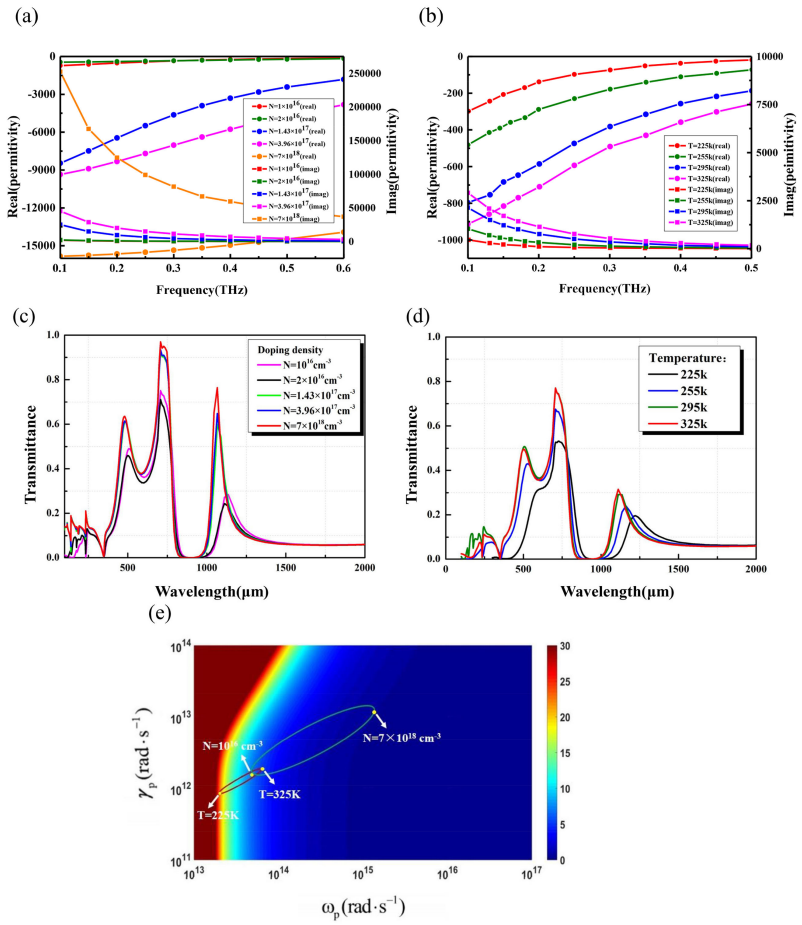

Fig. 2. (a) The real part and imaginary part of the permittivity of InSb at different carrier concentration. (b) The real part and imaginary part of the permittivity of InSb at different temperature. (c) The transmittance $T(\lambda)$ as a function of doping density, which changes from 10^{16} cm^{-3}(intrinsic InSb), 2×10^{16} cm^{-3}, 1.43×10^{17} cm^{-3}, 3.96×10^{17} cm^{-3} to 7×10^{18} cm^{-3}. (d) The transmittance $T(\lambda)$ as a function of temperature, which changes from 225 k, 255 k, 295 k to 325 k. (e) The skin depth of InSb material in different temperature and doping density. The red ellipse corresponds to the region of intrinsic InSb with different temperature, the green ellipse corresponds to the region of InSb with different doping density.

Where $\varepsilon_\infty = 15.7$ is the high-frequency permittivity, $\tau = \mu m^*/e$ is the average collision time of the charge carriers and $\omega_p = \sqrt{Ne^2/\varepsilon_\infty \varepsilon_0 m^*}$ is the plasma frequency. N represents the semiconductor charge carrier concentration and μ represents the carrier mobility, while e is the fundamental charge, ε_0 the vacuum permittivity, $m*$ the charge carrier effective mass and $m* = 0.014\ m_0$, where m_0 is the electron mass. It is known that $\omega_{\rm p}$ and τ vary with temperature T and the doping concentration N. For example, when T = 295 k, $\omega_{\rm p} = 5 \times 10^{13}$ Hz and $\tau = 6.17 \times 10^{-13}$ s, when N = 7×10^{18} cm^{-3}, $\omega_{\rm p} = 1.26 \times 10^{15}$ Hz and $\tau = 1 \times 10^{-13}$ s [35]–[41]. As illustrated in Fig. 2(a) and 2(b), the real part and imaginary part of the permittivity of InSb at different carrier concentration and different temperature are calculated respectively. It can be observed that the absolute value of the permittivity of InSb with different temperature and different carrier concentration at THz frequencies is much lower than that of metal like gold, which is more than 105. It is known that holes do not contribute to the metallic character of InSb. Because their mobility is much lower in comparison to the electron mobility, so the contribution of holes to the complex permittivity is negligible.

Fig. 2(c) and 2(d) illustrate the transmittance $T(\lambda)$ as a function of wavelength with different doping densities and different temperatures, respectively. From Fig. 2(c), it is clear that the transmittance enhances as the doping density N increases, and the data also shows the extraordinary transmittance effect that transmission of the order of 95% was found at $\lambda = 750$ μm when $N = 7 \times 10^{18}$cm^{-3}. We can conclude that the transmission of the doped InSb has increased by about 1.3 times compared to the intrinsic InSb. In Fig. 2(d), it also shows the overall increase of the transmittance $T(\lambda)$ as the temperature rises from 225 k to 325 k. At 325 k, a pronounced peak at a wavelength about 750 μm is obtained, and the maximum can reach about 0.8 which is 1.5 times higher than that at lower temperature 225 k. These two results demonstrate that the transmission properties of InSb grating structure can be easily tuned by changing the temperature or doping density N. For further explanation, the skin depth of InSb material in different temperature and doping density are compared in Fig. 2(e). The value of the skin depth of electromagnetic waves is determined by the optical field penetration depth in InSb. As it can be concluded from the Drude model, the temperature and carrier density also have effect on the scattering rate, which changes the skin depth directly. The red and the green circles show the regions of photoexcited InSb with various temperatures and doping densities, respectively. It is noticed that as the temperature increases from 225 K to 325 K, the skin depth varies from 27.79 to 5.32 μm, and with the increase of doping density from 10^{16} cm^{-3} to 7×10^{18} cm^{-3}, the skin depth decreases from 7.43 to 0.48 μm. This is consistent with the transmission results at different temperatures and different doping densities. With the increase of the temperature and the doping density, the depth of light penetration into the grating structure reduces, causing the effective size of the groove decreases and the coupling of the incident radiation decreases with smaller effective refractive index. Therefore, the transmission through the grating structure has an obvious enhancement. In summary, in order to obtain the optimized transmission result, the doping concentration is set to $N = 7 \times 10^{18}$ cm^{-3} in the following simulations and the temperature is set to 295 k.

To lay the foundations for the discussion of the enhanced transmission, we review the basic physics of the transmission of light through a single hole in an aperture. Since the transmission process is accompanied by diffraction, various approximations developed in classical diffraction theory was used in the simulation [6]. Next, the influence of the position of patterning grooves on transmission was investigated. The array of the aperture is considered infinite and periodic in the simulation process to simplify the theoretical analysis of the optical response. Therefore, only EM fields within one unit cell need to be computed with the help of Bloch's theorem. A variety of 3-dimensional arrays of different structure were set up to analyze the relationship between the transmission T and the position of the grooves, and the results are shown in Fig 3(a). These four structures have the same grating period $d = 300$ μm, the groove depth $h_1 = 100$ μm and the width $w = 100$ μm. Notation [M_{I}, M_{O}] means $2M_{\mathrm{I}}$ grooves in the input surface and $2M_{\mathrm{O}}$ grooves in the output surface. In both surfaces, grooves are located symmetrically around the central slit. The spectrum shows a number of distinct features. The curve for [0, 0] corresponds to the case with a single slit, and its $T(\lambda)$ only presents two maxima in this frequency range while the other three cases all present three maxima. This phenomenon indicates that these two peaks around 500 μm and 1150 μm are only associated to the excitation of slit waveguide resonances [19], [20], [42], which is excited by the coupling of incident waves with waveguide resonances located in the slits. An extra peak at $\lambda \approx 750$ μm can be observed in the spectrum of another three cases: [0, 10], [10, 0] and [10, 10]. The excitation of an EM resonance at the corrugated input grating surface, originated by the interplay between the groove cavity mode and the in-phase groove reemission mechanisms is responsible for the extra peak [19]. It can also be obtained from Fig. 3(a) that the maximum transmission occurs at the curve for [10, 10] and the absolute transmission efficiency almost reaches 80%. Therefore, in order to obtain the maximum transmission efficiency, a structure with grooves on both surfaces should be adopted. For a further explanation on the impact of different groove positions, the dependency of transmission and groove depth for the case of [10, 0] and [0, 10] are shown in Fig. 3(b) and 3(c), respectively. As we can see from Fig. 3(b), the overall transmission increases as the grating depth h_1 varies from 20 μm to 100 μm, which indicates that the depth of the upper groove has more significant influence on the transmission. In contrast,

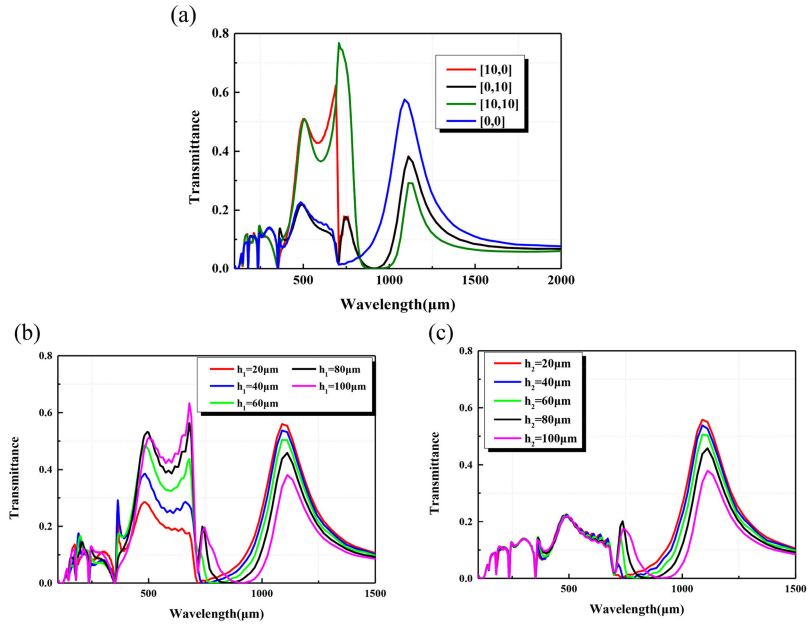

Fig. 3. (a) The transmittance $T(\lambda)$ of four different InSb grating structure at THz frequency. Geometrical parameters used in the figures are $w = 100$ μm, $d = 300$ μm, $H = 400$ μm, and the depth of the grooves $h1 = h2 = 100$ μm. Notation [M_I, M_O] means $2M_I$ grooves in the input surface and $2M_O$ grooves in the output surface. In both surfaces, grooves are located symmetrically around the central slit. (b) The dispersion relations of SPPs in one unit of the designed InSb grating waveguides with different groove position. The transmittance $T(\lambda)$ as a function of the groove depth in (c) input surface and (d) output surface.

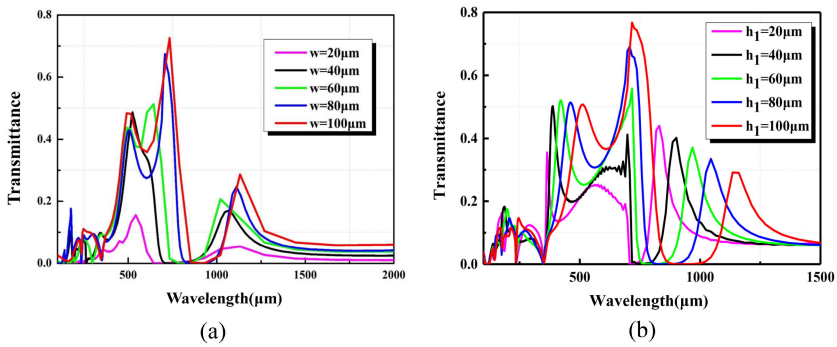

Fig. 4. (a) The transmittance $T(\lambda)$ as a function of the groove width on the input surface which changes from 20 μm to 100 μm. (b) The transmittance $T(\lambda)$ as a function of the groove depth on the input surface which changes from 20 μm to 100 μm.

Fig. 3(c) shows a weaker variation of the THz transmission through InSb with the output surface groove depth h_2. Especially at the range 0–800 μm, the transmission remains basically the same as the depth changes. It can be drawn that the transmission is mainly controlled by the pattern on the input corrugation while the grooves on the output surface only have a weaker impact on the transmission especially at larger wavelength. Therefore, in the subsequent simulation, we mainly study the influence of the structural parameters of the input surface grooves on the transmission.

To elucidate the role of input groove geometrical parameters on the behavior of SPPs in the grating structure, the effect of different groove widths and depths on transmission are considered in Figure 4. As mentioned before, in order to obtain the optimized transmission result, grooves on the

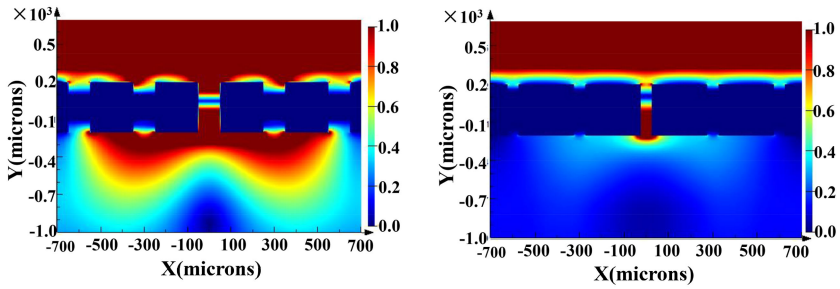

Fig. 5. (a) The light field profile of the structure with parameters $N = 7 \times 10^{18}$ cm^{-3}, $M_{\mathrm{I}} = M_{\mathrm{O}} = 10$, and $w = h_1 = 100$ μm. (b) The light field profile of the structure with parameters $N = 7 \times 10^{18}$ cm^{-3}, $M_{\mathrm{I}} = M_{\mathrm{O}} = 10$, and $w = h_1 = 50$ μm.

output surface were also kept, and its width $w = 100$ μm, depth $h_2 = 100$ μm. The other geometric parameters used in the simulation are $d = 300$ μm, $H = 400$ μm, and the number of the grooves on both sides is $M_{\mathrm{I}} = M_{\mathrm{O}} = 10$. As illustrated in Fig. 4(a), the transmission $T(\lambda)$ enhances with the increase of the groove width which changes from 20 μm to 100 μm and when $w > 40$ μm, the peak appears at a larger wavelength as the groove width increases. This phenomenon may be attributed to two effects: The first one arises from the fact that the SPP dispersion relationship is greatly depended on the surface groove structure. The second one is due to the coupling of SPPs on the internal interfaces of the slit, which increase the effective index for the cavity mode and then decrease the resonance frequency when the width increases [43]. When $w = 20$ μm, the light field transmitted through the grating remains low as the wavelength changes. There are only two visible peaks in the transmission curve when $w = 20$ and 40 μm and the peak around $\lambda = 750$ μm is disappeared. Based on what was demonstrated before, this missing peak is related to the grating-coupling at the periodic aperture. It can be inferred that due to the extremely narrow width of the groove, the excitation of a surface EM resonance originated from the interplay between the groove cavity mode and the in-phase groove reemission mechanism is not conspicuous. Similarly as Fig. 4(a), the peak around 750 μm become less noticeable when the groove depth $h_1 = 20$ μm in Fig. 4(b). In addition, there is a distinct tendency that the transmission $T(\lambda)$ enhances with deeper grooves. When $h_1 = 100$ μm, the maximum can reach almost 0.8 near the wavelength $\lambda = 750$ μm, which increases nearly 4 times compared to the case $h_1 = 20$ μm. Also it can be seen from Fig. 4(b) is the redshift of the peak position as the depth of grooves increases from the first peak. This phenomenon implies that we can flexibly obtain the desired peak by adjusting the groove width and depth [44], [45]. In general, in order to obtain the highest transmission efficiency, the grating structure with a groove width and depth of 100 μm is the best choice.

Based on the above analysis of the transmission results for different grating structure, a set of parameters of the highest transmission efficiency can be obtained. The known optimal combination of parameters is the doping concentration of InSb $N = 7 \times 10^{18}$ cm^{-3}, $M_{\mathrm{I}} = M_{\mathrm{O}} = 10$, $w = h_1 = 100$ μm and the temperature is set to 325 k. To further elucidate the role of the set of parameters on transmission enhancement effect, the light passing through the optimal parameter structure and the common structure at the same wavelength $\lambda = 750$ μm was compared by the light field profile. The comparison diagrams are shown in Fig. 5. Fig. 5(a) illustrates the light field distribution for the structure with optimal parameters and Fig. 5(b) displays the light field for the structure with $N = 7 \times 10^{18}$ cm^{-3}, $M_{\mathrm{I}} = M_{\mathrm{O}} = 10$, $w = h_1 = 50$ μm and the temperature is set to 295 k. The spectrum results show a number of distinct features, and the most remarkable part is that the light tunneling through the first structure far exceeds the light passing through the second structure. In addition, Fig. 5(a) also indicates that the electric fields are most intense at the corner of the ridges. For this reason one considers the first structure to give stronger coupling between the incident light and the grooves, and therefore a more obvious SPPs effect. There are two kinds of

SPP resonance modes for the grating surface of the rectangular unit. One is the horizontal surface plasmon resonance (HSPR) existing on the upper and corner of the grooves like the concentration of beams shown in Fig. 5(a), which is a resonance mode induced by a horizontal periodic structure; the other is the vertical surface plasmon resonance (VSPR) existing on the left and right vertical surfaces of the grooves and it is a kind of Fabry-Perot resonance mode [46]. It is generally admitted that the presence of HSPR increases the stronger horizontal resonance between adjacent grooves and VSPR allows the enhanced light field generated by the coupling to transfer farther in the *z* direction. However, some researchers hold the idea that SPPs paly the negative role for the extraordinary transmission, and Cao and Lalanne consider the high transmission is generated from waveguide-mode resonance and diffraction [47]. They have shown that the transmission is nearly zero at the SPP excitation wavelength, and the wavelength λ_{SP} is given by:

$$\lambda_{\mathrm{SP}} = \frac{d}{n}\left[\mathrm{Re}\left\{\left[\varepsilon/\left(1+\varepsilon\right)\right]^{1/2}\right\} \pm \sin\left(\theta\right)\right] \tag{2}$$

Where θ represents the angle of incidence, *n* is a nonzero relative integer. In our simulation, the calculated λ_{SP} equals to 382.3 μm when $\theta = 0°$ and $n = 1$. It can be seen from Fig. 2(c) that the transmission is extremely weak at $\lambda = 382.3$ μm, which is consistent with the view of Cao and Lalanne. Therefore, the mechanism of the extraordinary transmission remains in dispute and still requires further research.

In addition to the EOT phenomenon, the focusing effect also appears in the grating structure we designed, and it only occurs within a very narrow range of wavelengths around the resonant condition. This phenomenon can be understood by assuming a SPP spreading along the grating from the exit side of the aperture towards both sides and then undergoing the directional emission at specific phase and amplitude [26]. The interference of the light emerging from the aperture will focusing at the point where the phase difference $\Delta\varphi = 2m\pi$ ($m = 1, 2, 3\ldots$), which is defined by the groove geometric parameters. The tuning of light through a subwavelength aperture can be significantly enhanced by patterning the input surface of the slit grating, which has been illustrated in detail. In a similar way, the emission on the output surface of the slit grating can be controlled via output surface patterning as well. We have learned that there are two conditions leading to large E-field intensity along the x-direction near the output surface [23]. One is the excitation of single groove cavity modes which is controlled by the groove width and depth, the other is the excitation of in-phase coupling between indentations which is stronger at $\lambda \approx d$. The lensing ability has been discussed by controlling the width of the slit, the depth of the grooves, and the period of the array at the output corrugation in previous studies [21]. In this letter, we set a model to investigate how the number and the depth of the groove influence the E-field intensity and focal length (distance from the output surface to the surface of a maximum E-field intensity). For the beaming properties only depend on the geometrical parameters defining the output surface, we remain other parameters $H = 400$ μm, $M_{\mathrm{I}} = 10$, $w = h_1 = 100$ μm, and $d = 300$ μm as before in our simulation. Fig. 6(a) displays the corresponding electric field intensity profile for the case $h_2 = 100$ μm and $M_{\mathrm{O}} = 10$ at the resonant wavelength $\lambda = 520$ μm. At the far-field region, a highly collimated beam with a very low divergence is observed. It can be seen clearly that there is a focusing effect associated with the beaming phenomenon. The localized SPPs focus the electromagnetic field at sub-wavelength scales leading to local field intensity enhancements of several orders of magnitude [21]. By cutting along the line of maximum E-field intensity ($z = 300$ μm) in panel Fig. 6(a), the E-field intensity at different wavelength λ along the *x*-direction is shown in Fig. 6(b). Consistent with Fig. 6(a), there are abrupt increases of the electric field in the middle of the grating at all the wavelength we set. In addition, the electric field intensity diffracted by the SPP wave at different wavelength varies greatly, and the light coupled into the SPP wave most efficiently only at one optimal wavelength. In our simulation, the optimal wavelength λ equals to 520 μm and its beaming intensity almost reaches 0.85 v/m, which is twice of that of $\lambda = 400$ μm. Therefore, the most intense focusing result can be achieved by changing the wavelength of the incident light.

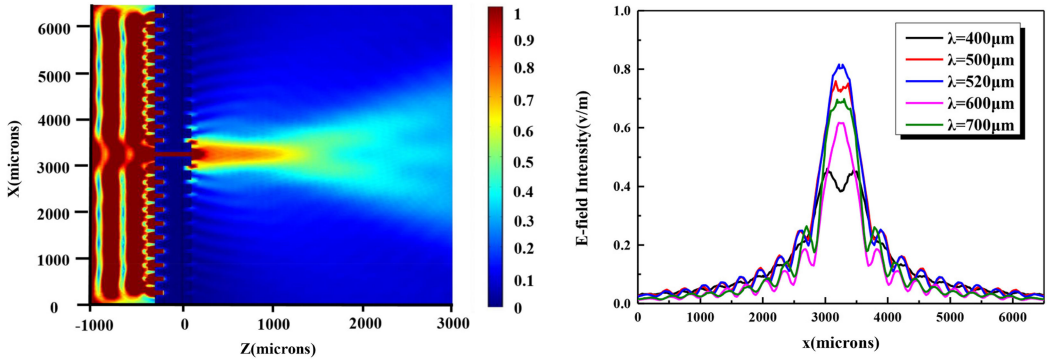

Fig. 6. (a) E-field intensity profile as a function of x and z for the case $N_{\mathrm{O}} = 10$, $d = 300$ μm, $w = 100$ μm and $h_2 = 100$ μm for the resonant $\lambda_{\mathrm{R}} = 520$ μm. (b) The E-field intensity along the x-direction cutting by the line of maximum E-field intensity ($z = 300$ μm) at different wavelength λ.

The process of light passing through the grating and focusing at a distance can be explained as follows: the primary beam is diffracted from the output corrugation through evanescent modes and the grooves diffract radiation either to outside or into other indentations immediately. Finally, a consistent EM field is built up at the output surface while the light reemitted into the vacuum [23]. As illustrated before, one of the conditions leading to large E-field intensity is the excitation of single groove cavity modes which is controlled by the output groove depth h_2. Therefore, for the fixed d, w, and M_{o}, there is an optimal h_2 to maximize E-field intensity, and an apparent focusing effect could be observed at a resonant wavelength λ_{R}. The dependence of E-field intensity on groove depth h_2 is summarized in Fig. 7. Figure 7(a) illustrates the calculated electric field intensity distribution of different groove depth along the x axis at the output surface. Note that the beam intensity at the middle of the grating has a strong correlation with h_2 and the maximum intensity almost reaches 0.8 v/m when $h_2 = 80$ μm. Figures 7(b)–(d) illustrate the corresponding $|\mathrm{H_y}|^2$ intensity distributions for $h_2 = 50$ μm, 80 μm and 150 μm at $\lambda = 510$ μm. It can be easily deduced from the comparison that the energy emerging from the slit and concentrating most of the energy in an extremely small region. An extrapolation of the figures is that the focal length also experiences variation with deeper groove depth. For example, the groove depth $h_2 = 50$ μm case shown in Fig. 7(b) reveals the focal length of 174 μm. When the depth increases to 80 μm, the focal length will lengthen to 610 μm. To summarize, the beaming intensity reaches the maximum 0.85 v/m when the wavelength $\lambda = 520$ μm, and the focal length up to 610 μm when $h_2 = 80$ μm in our simulation. From the results, conclusions can be made that we have revealed the beaming effect in the output region, and we have proposed a focal length modulation method of simply tuning the groove depth or wavelength. These investigations of the property of the beam provide new theoretical approaches to controlling light in special nano optical applications, such as optical microprobes and coupler.

In order to investigate the influence of the output surface groove number on focal length, we simulate the $|\mathrm{H_y}|^2$ intensity distribution profile of different M_{o} with the wavelength changes from 460 to 660 μm to obtain the corresponding focal lengths, and the result is shown in Fig. 8. The other parameters are set as $d = 300$ μm, $w = h_2 = 100$ μm, and $\lambda = 510$ μm. As it can be seen from the figure, the focal length does not necessarily increase when increasing M_{o}. When $\lambda = 560$ μm, the calculation gives that the maximum variation of the focal length by adding grooves to the grating is about 5%. This invariance is due to the mechanism of the focusing effect: excitation of single groove cavity modes and in-phase coupling between indentations, which has little connection with the output groove number M_{o}. Furthermore, the effective tuning of the focal length is accomplished through modulating the exit relative phase distribution, and the phase distribution of the transmitted beam is only related to the depth of the groove, regardless of the number of output grooves. In summary, the position and length of the focus are independent of the number of the output groove,

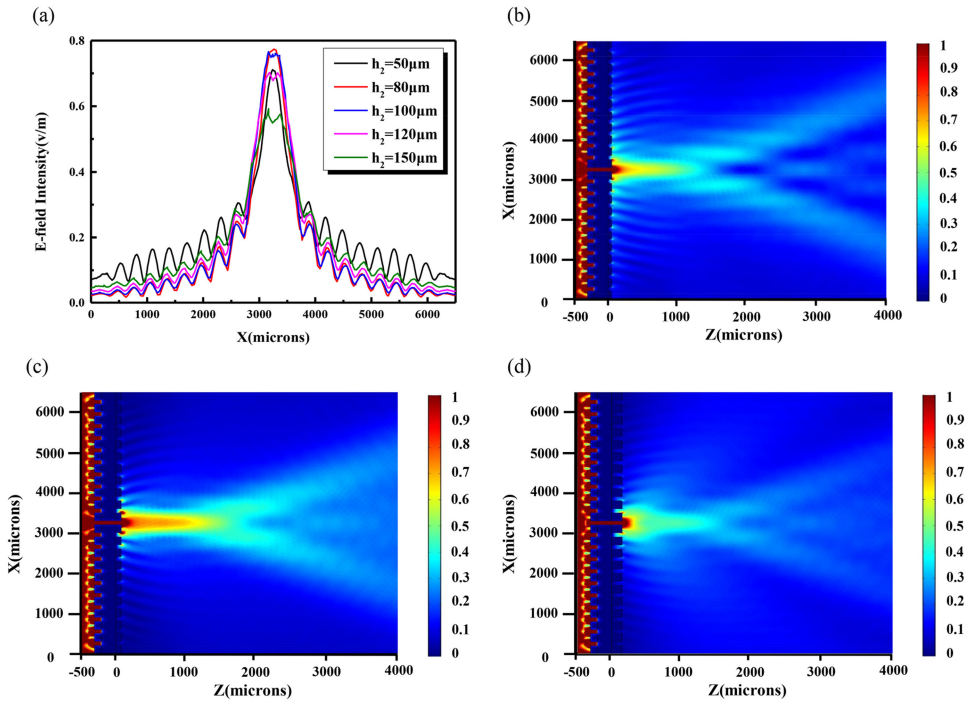

Fig. 7. (a) The E-field intensity along the x-direction by the line of z is 300 μm away the output surface at different groove depth h_2 for the case $N_{\rm O} = 10$, $d = 300$ μm and $w = 100$ μm for the resonant $\lambda_{\rm R} = 510$ μm. The E-field intensity profile as a function of x and z at a groov e depth of (b) $h_2 = 50$ μm, (c) $h_2 = 80$ μm and (d) $h_2 = 150$ μm.

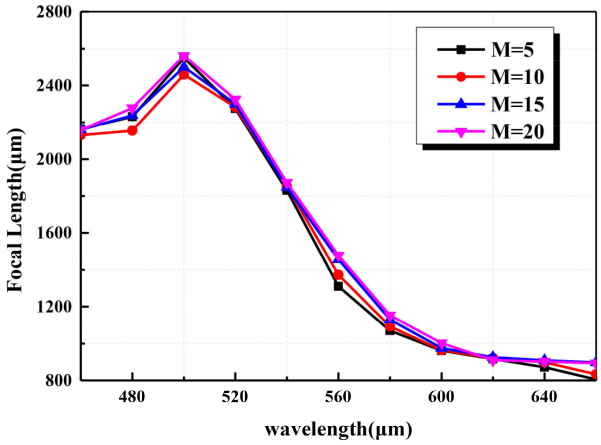

Fig. 8. The focal length as a function of wavelength at different output groove number. $M_{\rm o}$ changes from 5, 10, 15 to 20 and the other parameters are fixed: $d = 300$ μm, $w = h_2 = 100$ μm, and $\lambda = 510$ μm.

and the light passing through the structure with different $M_{\rm o}$ could be focused at the same spot in the output region.

4. Conclusions

In this work, the properties of the extraordinary optical transmission (EOT) phenomenon and the beaming effect have been analyzed successfully by tuning the pattern on the input and

output corrugation of the InSb slit waveguide, respectively. By means of altering the temperature, doping concentration of InSb and the geometrical parameters of the input corrugation, the greatly enhanced transmission are obtained and the maximum transmission efficiency reaches 95%. The properties of the beaming intensity and focal length are thoroughly analyzed by changing the number and depth of the output groove at a fixed wavelength. And the results show that the maximum of the beaming intensity reaches 0.85 v/m, which is twice the minimum value. The investigations of the unique SPPs properties of the InSb slit grating structure we designed pave the way towards a wide range of novel applications in future plasmonic devices at THz range. For example, the high transmission efficiency property inspire designs for enhanced devices such as near-field scanning optical microscopes and ultra-high density optical data storage devices. In addition, in practical applications, the tunability of the resonant wavelength improves the flexibility of these devices. At the same time, the beaming effect can be applied to the devices that can transmit or receive light along a specific direction for a given wavelength, such as the spectral multiplexing and the fiber coupling. In summary, our findings demonstrates a way to break through traditional optical diffraction limitations and these theoretical analysis lay the foundation for further application of optical devices.

References

[1] J. Gómez Rivas, M. Kuttge, H. Kurz, P. H. Bolivar, and J. A. Sánchez-Gil, "Low-frequency active surface plasmon optics on semiconductors," *Appl. Phys. Lett.*, vol. 88, no. 8, 2006, Art. no. 082106.

[2] P. Berini, "Plasmon-polariton modes guided by a metal film of finite width," *Opt. Lett.,* vol. 24, no. 15, pp. 1011–1013, 1999.

[3] R. Y. Kangyang *et al.*, "Rainbow trapping and releasing in InSb graded subwavelength grooves by thermal tuning at the terahertz range," *Opt. Mater. Exp.*, vol. 8, no. 9, pp. 2954–2966, 2018.

[4] T. W. Ebbesen, H. J. Lezec, H. F. Ghaemi, T. Thio, and P. A. Wolff, "Extraordinary optical transmission through sub-wavelength hole arrays," *Nature*, vol. 391, no. 6688, pp. 667–669, 1998.

[5] L. Martin-Moreno *et al.*, "Theory of extraordinary optical transmission through subwavelength hole arrays," *Phys. Rev. Lett.*, vol. 86, no. 6, pp. 1114–1117, 2001.

[6] H. J. Lezec *et al.*, "Beaming light from a subwavelength aperture," *Science*, vol. 297, no. 5582, pp. 820–822, 2002.

[7] A. Krishnan *et al.*, "Evanescently coupled resonance in surface plasmon enhanced transmission," *Opt. Commun.*, vol. 200, pp. 1–7, 2001.

[8] E. Popov, M. Neviere, S. Enoch, and R. Reinisch, "Theory of light transmission through subwavelength periodic hole arrays," *Phys. Rev. B*, vol. 62, no. 23, pp. 16100–16108, 2000.

[9] L. Salomon, F. Grillot, A. V. Zayats, and F. de Fornel, "Near-field distribution of optical transmission of periodic subwavelength holes in a metal film," *Phys. Rev. Lett.*, vol. 86, no. 6, pp. 1110–1113, 2001.

[10] V. A. Shubin, A. K. Sarychev, J. P. Clerc, and V. M. Shalaev, "Local electric and magnetic fields in semicontinuous metal films: Beyond the quasistatic approximation," *Phys. Rev.*, vol. 62, no. 16, pp. 11230–11244, 2000.

[11] J. A. Porto, F. J. Garcia-Vidal, and J. B. Pendry, "Transmission resonances on metallic gratings with very narrow slits," *Phys. Rev. Lett.*, vol. 83, no. 14, pp. 2845–2848, 1999.

[12] S. Collin, F. Pardo, R. Teissier, and J. L. Pelouard, "Strong discontinuities in the complex photonic band structure of transmission metallic gratings," *Phys. Rev. B*, vol. 63, no. 3, 2001, Art. no. 033107.

[13] J. M. Vigoureux, "Analysis of the Ebbesen experiment in the light of evanescent short range diffraction," *Opt. Commun.*, vol. 198, no. 4–6, pp. 257–263, 2001.

[14] H. E. Went, A. P. Hibbins, J. R. Sambles, C. R. Lawrence, and A. P. Crick, "Selective transmission through very deep zero-order metallic gratings at microwave frequencies," *Appl. Phys. Lett.*, vol. 77, no. 18, pp. 2789–2791, 2000.

[15] Y. Takakura, "Optical resonance in a narrow slit in a thick metallic screen," *Phys. Rev. Lett.*, vol. 86, no. 24, pp. 5601–5603, 2001.

[16] F. Z. Yang and J. R. Sambles, "Resonant transmission of microwaves through a narrow metallic slit," *Phys. Rev. Lett.*, vol. 89, no. 6, 2002, Art. no. 063901.

[17] A. Barbara, P. Quemerais, E. Bustarret, and T. Lopez-Rios, "Optical transmission through subwavelength metallic gratings," *Phys. Rev. B*, vol. 66, no. 16, 2002, Art. no. 161403.

[18] A. P. Hibbins, J. R. Sambles, and C. R. Lawrence, "Gratingless enhanced microwave transmission through a subwavelength aperture in a thick metal plate," *Appl. Phys. Lett.*, vol. 81, no. 24, pp. 4661–4663, 2002.

[19] F. J. Garcia-Vidal, H. J. Lezec, T. W. Ebbesen, and L. Martin-Moreno, "Multiple paths to enhance optical transmission through a single subwavelength slit," *Phys. Rev. Lett*, vol. 90, no. 21, 2003, Art. no. 213901.

[20] D. C. Skigin and R. A. Depine, "Transmission resonances of metallic compound gratings with subwavelength slits," *Phys. Rev. Lett.*, vol. 95, no. 21, 2005, Art. no. 217402.

[21] F. J. Garcia-Vidal, L. Martin-Moreno, H. J. Lezec, and T. W. Ebbesen, "Focusing light with a single subwavelength aperture flanked by surface corrugations," *Appl. Phys. Lett.*, vol. 83, no. 22, pp. 4500–4502, 2003.

[22] J. G. Rivas, C. Janke, P. H. Bolivar, and H. Kurz, "Transmission of THz radiation through InSb gratings of subwavelength Apertures," *Opt. Exp.*, vol. 13, no. 3, pp. 847–859, 2005.

[23] L. Martin-Moreno, F. J. Garcia-Vidal, H. J. Lezec, A. Degiron, and W. W. Ebbesen, "Theory of highly directional emission from a single subwavelength aperture surrounded by surface corrugations," *Phys. Rev. Lett.*, vol. 90, no. 16, 2003, Art. no. 167401.
[24] L. B. Yu, D. Z. Lin, Y. C. Chen, Y. C. Chang, K. T. Huang, and J. W. Liaw, "Physical origin of directional beaming emitted from a subwavelength slit," *Phys. Rev. B*, vol. 71, no. 4, 2005, Art. no. 041405.
[25] Y. Lee, K. Hoshino, A. Andrea, and X. Zhang, "Efficient directional beaming from small apertures using surface-plasmon diffraction gratings," *Appl. Phys. Lett.*, vol. 101, no. 4, 2012, Art. no. 041102.
[26] H. F. Shi, C. L. Du, and X. G. Luo, "Focal length modulation based on a metallic slit surrounded with grooves in curved depths," *Appl. Phys. Lett*, vol. 91, no. 9, 2007, Art. no. 093111.
[27] M. A. Seo *et al.*, "Terahertz field enhancement by a metallic nano slit operating beyond the skin-depth limit," *Nature Photon.*, vol. 3, no. 3, pp. 152–156, 2009.
[28] A. Berrier, R. Ulbricht, M. Bonn, and J. G. Rivas, "Ultrafast active control of localized surface plasmon resonances in silicon bowtie antennas," *Opt. Exp.*, vol. 18, no. 22, pp. 23226–23235, 2010.
[29] J. Gómez Rivas, C. Schptsch, P. Haring Bolivar, and H. Kuez, "Enhanced transmission of THz radiation through sub-wavelength holes," *Phys. Rev. B*, vol. 68, no. 20, 2003, Art. no. 201306.
[30] C. Janke, J. Gómez Rivas, C. Schotsch, L. Beckmann, P. H. Bolivar, and H. Kurz, "Optimization of the enhanced THz transmission through arrays of sub-wavelength apertures," *Phys. Rev. B*, vol. 69, 2004, Art. no. 205314.
[31] J. Gómez Rivas, C. Schotsch, P. H. Bolivar, and H. Kurz, "Thermal switching of the enhanced transmission of THz radiation through sub-wavelength apertures," *Phys. Rev. B*, vol. 68, 2003, Art. no. 201306.
[32] B. S. Passmore, D. G. Allen, S. R. Vangala, W. D. Goodhue, D. Wasserman, and E. A. Shaner, "Mid-infrared doping tunable transmission through subwavelength metal hole arrays on InSb," *Opt. Exp.*, vol. 17, no. 12, pp. 10223–10230, 2009.
[33] D. E. Grupp, H. J. Lezec, T. W. Ebbesen, K. M. Pellerin, and T. Thin, "Crucial role of metal surface in enhanced transmission through subwavelength apertures," *Appl. Phys. Lett.*, vol. 77, no. 11, pp. 1569–1571, 2000.
[34] M. Van Exter, "Optical and electronic properties of doped silicon from 0.1 to 2 THz," *Appl. Phys. Lett.*, vol. 56, no. 17, pp. 1694–1696, 1990.
[35] S. M. Hanham *et al.*, "Broadband terahertz plasmonic response of touching InSb disks," *Adv. Mater.*, vol. 24, no. 35, pp. 226–229, 2012.
[36] F. Kuchar, E. Fantner, and G. Bauer, "Doping dependence of high-field donor spectra in InSb," *Solid State. Phys.*, vol. 10, no. 18, pp. 3577–3587, 1977.
[37] J. T. McMahon and R. J. Bell, "Infrared reflectivity of doped InSb and CdS," *Phys. Rev.*, vol. 182, no. 2, pp. 526–530, 1969.
[38] W. E. Anderson, R. W. Alexander, and R. J. Bell, "Surface plasmons and the reflectivity of n-Type InSb," *Phys. Rev. Lett.*, vol. 27, no. 16, 1966, Art. no. 271057.
[39] P. P. Paskov, "Refractive indices of InSb, InAs, GaSb, InAsxSb1−x, and In1−xGaxSb: Effects of free carriers," *J. Appl. Phys.*, vol. 81, pp. 1890–1898, 1997.
[40] X. Y. He, "Numerical analysis of the propagation properties of subwavelength semiconductor slit in the terahertz region," *Opt. Exp.*, vol. 17, no. 17, pp. 15359–15371, 2009.
[41] X. Wang, Y. Deng, and Q. Li, "Excitation and propagation of surface plasmon polaritons on a non-structured surface with a permittivity gradient," *Light: Sci. Appl.*, vol. 5, no. 12, 2016, Art. no. e16179.
[42] Z. J. Sun, Y. S. Jung, and H. K. Kim, "Role of surface plasmons in the optical interaction in metallic gratings with narrow slits," *Appl. Phys. Lett.*, vol. 83, no. 15, pp. 3021–3023, 2003.
[43] T. H. Isaac, J. Gómez Rivas, J. R. Sambles, W. L. Barnes, and E. Hendry, "Surface plasmon mediated transmission of subwavelength slits at THz frequencies," *Phys. Rev. B*, vol. 77, no. 11, 2008, Art. no. 113411.
[44] R. Gordon, "Light in a subwavelength slit in a metal: Propagation and reflection," *Phys. Rev. B*, vol. 3, no. 15, 2006, Art. no. 153405.
[45] S. Collin, F. Pardo, and J. L. Pelouard, "Waveguiding in nanoscale metallic apertures," *Opt. Exp.*, vol. 15, no. 7, pp. 4310–4320, 2007.
[46] S. Collin, F. Pardo, R. Teissier, and J. L. Pelouard, "Horizontal and vertical surface resonances in transmission metallic gratings," *J. Opt. A: Pure Appl. Opt.*, vol. 4, no. 5, pp. 154–160, 2002.
[47] Q. Cao and P. Lalanne, "Negative role of surface plasmons in the transmission of metallic gratings with very narrow slits," *Phys. Rev. Lett.*, vol. 88, no. 5, 2002, Art. no. 57403.